

Supplementary Materials

Tuning the Co Oxidation State in $\text{Ba}_{0.5}\text{Sr}_{0.5}\text{Co}_{0.8}\text{Fe}_{0.2}\text{O}_{3-\delta}$ by Flame Spray Synthesis towards High Oxygen Evolution Reaction Activity

Dino Aegerter ^{1,*}, Mario Borlaf ², Emiliana Fabbri ^{1,*}, Adam H. Clark ¹, Maarten Nachtegaal ¹,
Thomas Graule ² and Thomas J. Schmidt ^{1,3}

¹ Energy and Environment Research Division, Paul Scherrer Institute PSI, Forschungsstrasse 111, CH-5232 Villigen PSI, Switzerland; adam.clark@psi.ch (A.H.C.); maarten.nachtegaal@psi.ch (M.N.); thomasjustus.schmidt@psi.ch (T.J.S.)

² Laboratory for High Performance Ceramics, Empa - Swiss Federal Laboratories for Materials Science and Technology, CH-8600 Dübendorf, Switzerland; marioborlaf@gmail.com (M.B.); thomas.graule@empa.ch (T.G.)

³ Laboratory of Physical Chemistry, ETH Zurich - Swiss Federal Institute of Technology in Zurich, CH-8093 Zürich, Switzerland;

* Correspondence: dino.aegerter@psi.ch (D.A.); emiliana.fabbri@psi.ch (E.F.);
Tel.: +41-56-310-5321 (D.A.); +41-56-310-2795 (E.F.)

S1. Transmission electron microscopy (TEM)

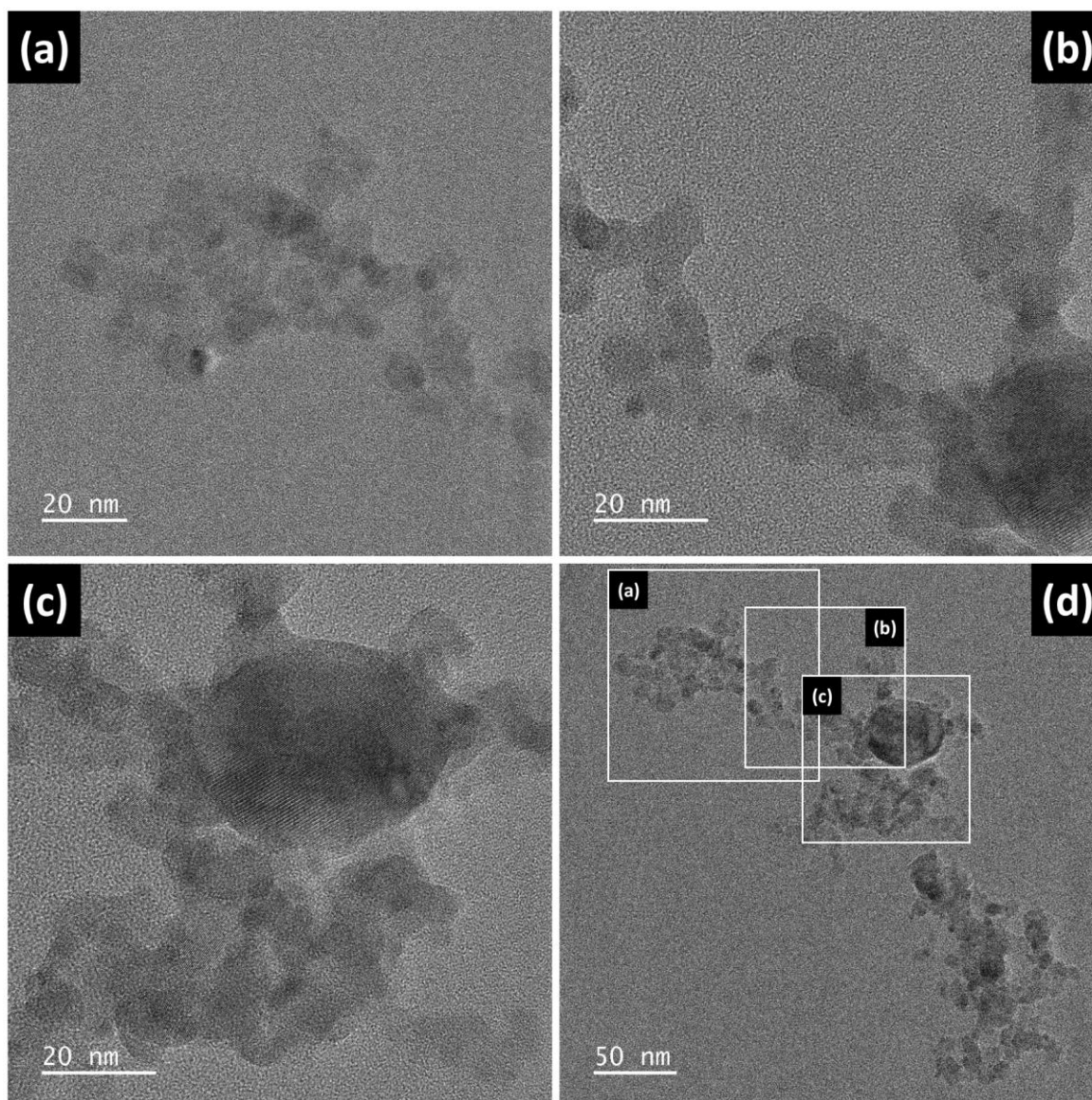


Figure S1. Transmission electron microscopy (TEM) images of the common BSCF batch—the batch which is in common for all three synthesis parameter investigations—produced with a total metal concentration (C_{TM}) of 0.1 M, a flow rate of the precursor solution (FR_{PS}) of 50 mL·min⁻¹ and of the dispersing gas (FR_{DG}) of 25 L·min⁻¹ exemplary for the bigger nanoparticles ((c) ~50 nm) seen in all BSCF batches.

S2. Powder X-ray diffraction (XRD)

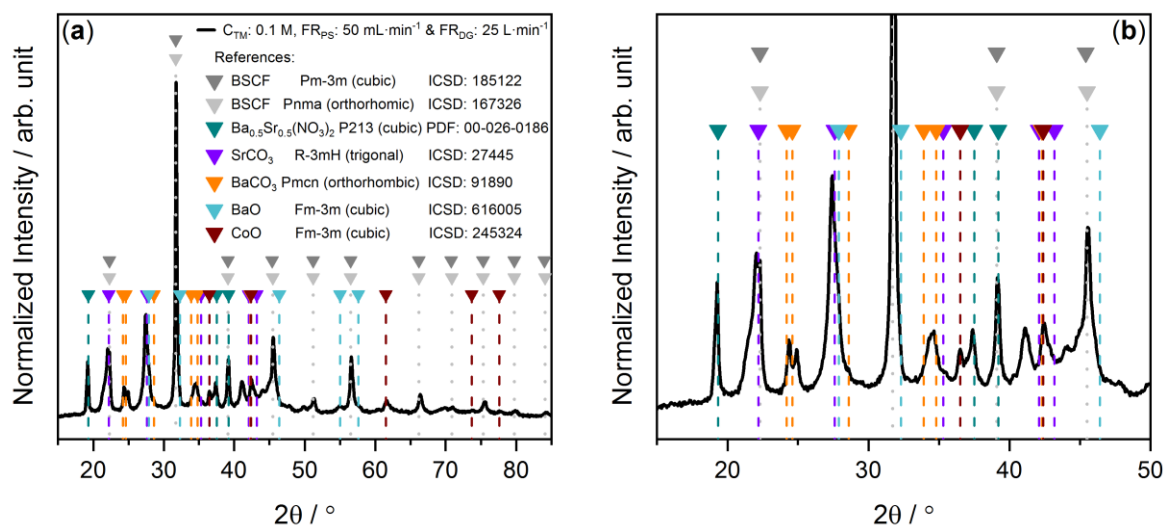


Figure S2. Comparison of the X-ray diffraction (XRD) pattern of the common BSCF batch ($C_{TM} = 0.1$ M, $FR_{PS} = 50$ mL \cdot min $^{-1}$ and $FR_{DG} = 25$ L \cdot min $^{-1}$)—the batch which is in common for all three synthesis parameter investigations—with BSCF and possible secondary phase references: (a) Same XRD pattern as the one shown at the bottom in Figure 2a, 3a and 4a in the article; (b) Magnification of (a) in the secondary phase dominated region.

The X-ray diffraction (XRD) pattern of the common BSCF batch ($C_{TM} = 0.1$ M, $FR_{PS} = 50$ mL \cdot min $^{-1}$ and $FR_{DG} = 25$ L \cdot min $^{-1}$)—the batch which is in common for all three synthesis parameter investigations—is shown representative for all BSCF batches in Figure S2 together with references of BSCF and of possible secondary phases. The primary phase of BSCF is overlapping well with the pattern of a cubic (\blacktriangledown ICSD: 185122) as well as an orthorhombic (\blacktriangledown ICSD: 167326) BSCF reference. The main difference between those two crystalline structures is that the length of all three axes of the unit cell are identical in the case of the cubic structure ($a = b = c$) but different in the case of the orthorhombic structure ($a \neq b \neq c$) while having in both cases the three angles of the unit cell identical ($\alpha = \beta = \gamma$). This leads to the consequences that the peaks assigned to the cubic structure are split in the case of the orthorhombic structure. However, such a splitting of the peaks is only resolved measurable when the width of these peaks are narrow and the splitting is strong enough. The used laboratory XRD device (refer to 4.2 Material Characterization in the article) and the particle size between 5-15 nm as shown in Figure 1 in the article (some particles up to 50 nm as shown in Figure S1) lead to a significant peak broadening which makes it impossible to distinguish the possible split peaks. Therefore, both crystalline structures are possible for the synthesized BSCF phase as indicated in Figure S2 with the two shown references.

Additional uncertainties occur when assigning the secondary phases of the flame spray synthesized BSCF batches, beside of the difficulties introduced by nanoparticles with having relative broad peaks. Possible secondary phases were assigned by limiting the possible elements in the phases to Ba, Sr, Co, Fe, O, C and N. This analysis showed that many materials could match with the peaks assigned to secondary phases. Therefore, the assigned secondary phases in Figure S2 is only one possibility among others. However, the occurrence of carbonates and nitrates in the flame spray synthesized BSCF batches is well known as secondary phases since the corresponding peaks of these highly water soluble species are missing after this type of flame spray synthesized materials are filtered and washed with ultrapure water [1]. This is a strong indication that many secondary phase peaks can be assigned to carbonates and nitrates. Nevertheless, a variety of carbonates and nitrates with different compositions could form secondary phases. A relative good overlap between secondary phase peaks and a nitrate reference is found for $Ba_{0.5}Sr_{0.5}(NO_3)_2$ (\blacktriangledown PDF:

00-026-0186) as shown in Figure S2. Moreover, SrCO_3 (▼ ICSD: 27445) and BaCO_3 (▼ ICSD: 91890) are well known carbonates in flame spray synthesized BSCF batches when using Ba or Sr nitrate precursors [1-3]. Possible is also mixtures of those two carbonates as $\text{Ba}_x\text{Sr}_{1-x}\text{CO}_3$ especially in the case with x close to one which could explain the slight offset towards smaller angles of the BaCO_3 (▼ ICSD: 91890) double peak at 25° in comparison to the measured XRD pattern. According to Bragg's law a partial replacement of Ba^{+2} in BaCO_3 with Sr^{+2} would lead to a shift of all peaks towards higher angles—assumed that the crystalline structure will remain with a low doping concentration—since Sr^{+2} atoms have a smaller diameter than Ba^{+2} atoms. However, no reference with a small doping amount was found in the used database. Moreover, several single oxides could also form secondary phases as BaO (▼ ICSD: 616005)—a possible intermediate in the BaCO_3 formation process [2]—or CoO (▼ ICSD: 245324). An overlap of the XRD patterns for the different synthesized BSCF batches showed that the peaks assigned to CoO as a possible secondary phase do not significantly change and thus cannot be the reason for the observed changes in the OER activity or Co oxidation state in BSCF as a function of the synthesis parameters.

S3. Co K-edge X-ray absorption near edge spectroscopy (XANES)

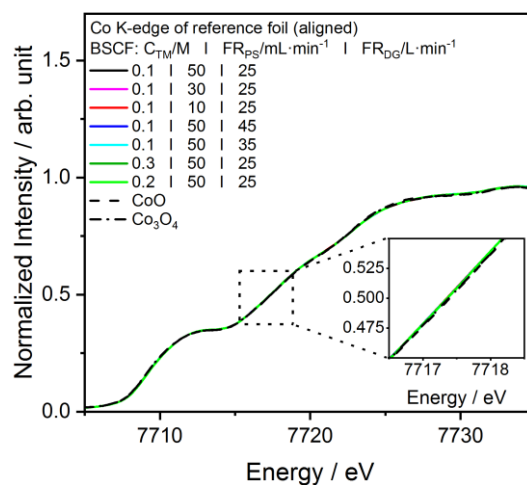


Figure S3. All aligned Co K-edge X-ray absorption near edge spectroscopy (XANES) spectra of the Co metal reference foil measured simultaneously with the samples and standards shown in Figure 2d, 3d and 4d in the article.

The XAS spectra were measured in transmission mode—a linear geometry—where the X-ray beam passes first the sample and then the reference foil. The beam intensity was measured first before the sample (I_0), then after passing the sample (I_1) and finally after passing the reference foil (I_2). Applying the natural logarithm on the division of the incident beam intensity (I_0) by the sample signal (I_1) results in the sample spectrum while applying the natural logarithm on the division of the sample signal (I_1) by the reference signal (I_2) results in the reference spectrum. Thus, there is for each sample spectrum a corresponding reference spectrum which was measured simultaneously. Both spectra were analyzed and processed in the same way. The reference spectra were used not only for the calibration of the energy scale but also for the comparison of different sample spectra measured in the same energy range—at the same edge. For the latter case, the reference spectra—measured with exactly the same foil—were aligned meaning that these spectra were shifted on the energy scale so that they all perfectly overlap. These energy shifts were then applied also to the corresponding sample spectra meaning that then these spectra will be aligned as well. These aligned sample spectra can then be plotted together as shown in Figure 2d, 3d and 4d in the article. Any observable energy shift at the same normalized intensity between the aligned sample spectra proves then the difference of the oxidation state of the measured element in those samples (Figure 2d, 3d and 4d). Moreover, the absence of any energy shift in the aligned reference spectra (Figure S3) proves that the energy shifts observed in the aligned sample spectra (Figure 2d, 3d and 4d) do not originate from any misalignment. Refer to 4.2 Material Characterization in the article for more information about the XAS measurement setup or to reference [4] for more information about the software used for the data processing.

S4. Fe K-edge XANES

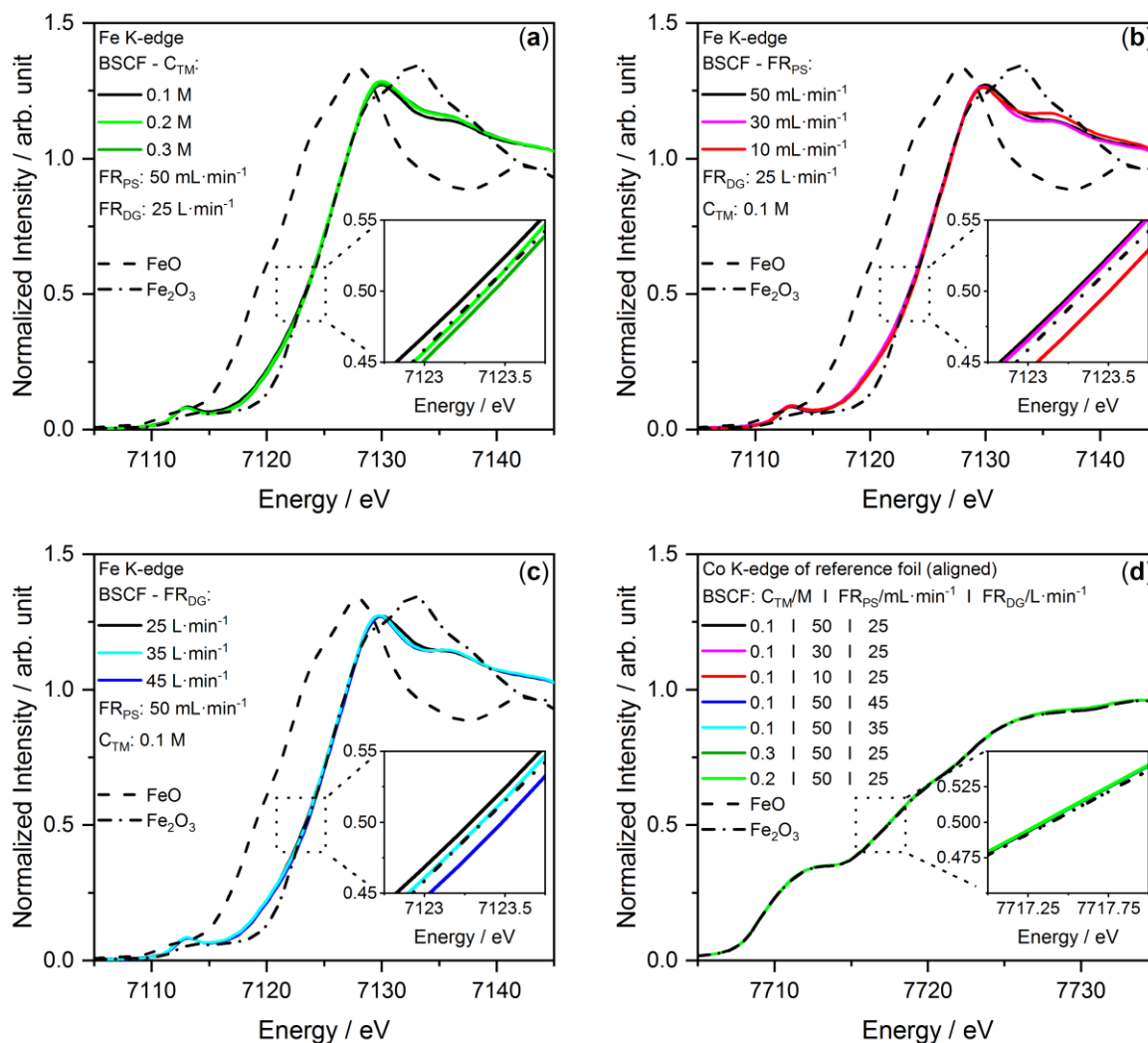


Figure S4. Comparison of Fe K-edge XANES spectra of the as-synthesized $Ba_{0.5}Sr_{0.5}Co_{0.8}Fe_{0.2}O_{3-\delta}$ (BSCF) batches produced to investigate (a) the total metal concentration (C_{TM}), (b) the flow rate of the precursor solution (FR_{PS}) and (c) the flow rate of the dispersion gas (FR_{DG}) as synthesis parameters (standards: Fe(II)O (---) and Fe(III)₂O₃ (-.-)). (d) All aligned Co K-edge XANES spectra of the Co metal reference foil measured simultaneously with the samples and standards shown in (a) - (c).

The Co and the Fe K-edge was measured simultaneously but only a Co foil was used as reference. Therefore, the Co reference foil spectra were also used for the alignment of the Fe K-edge spectra. Refer to S3 for a detailed explanation of the alignment process. In summary, even though the energy shifts at the same normalized intensity—observed in the Fe K-edges in Figure S4a, S4b and S4c—are relative small, are the shifts indeed real since no systematic trend is observable in the corresponding aligned reference spectra (Figure S4d).

S5. Reference electrode (RE) calibration

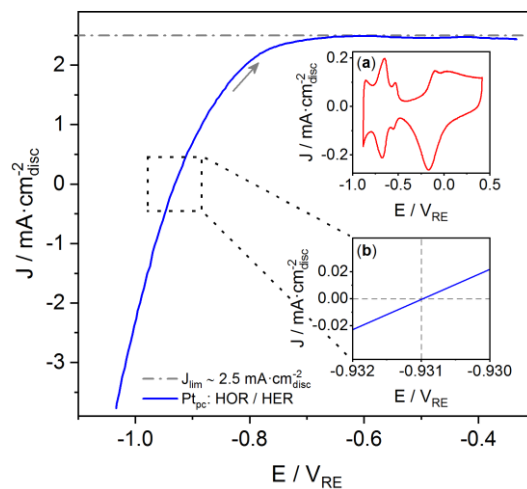


Figure S5. Recorded cyclic voltammograms (CVs) of a polycrystalline platinum disc insert (Pt_{pc}) for the reference electrode calibration in a 0.1 M potassium hydroxide (KOH) solution. Hydrogen oxidation reaction/Hydrogen evolution reaction (HOR/HER) polarization curve (—) measured with a scan rate of $20 \text{ mV}\cdot\text{s}^{-1}$ and a rotating disk electrode (RDE) speed rate of 1600 rpm while having the electrolyte saturated with H_2 . The arrow indicates that only the positive-going scan is shown here. A diffusion-limited current density (J_{lim}) of around $2.5 \text{ mA}\cdot\text{cm}^{-2}_{\text{disc}}$ (---) was reached which is in good agreement with [5-7]. Insets: (a) Measured before the calibration (—) with a scan rate of $100 \text{ mV}\cdot\text{s}^{-1}$ while having the electrolyte saturated with N_2 (RDE speed rate = 0 rpm); (b) HOR/HER polarization curve at the x-axis intercept ($J = 0 \text{ mA}\cdot\text{cm}^{-2}_{\text{disc}}$) showing the offset of the reference electrode (RE, Hg/HgO) versus the reversible hydrogen electrode (RHE) of +0.931 V which is opposite as seen in this inset since all shown potentials here are versus the used RE (V_{RE}).

References

1. Kim, B.J.; Fabbri, E.; Abbott, D.F.; Cheng, X.; Clark, A.H.; Nachtegaal, M.; Borlaf, M.; Castelli, I.E.; Graule, T.; Schmidt, T.J. Functional role of Fe-doping in Co-based perovskite oxide catalysts for oxygen evolution reaction. *J Am Chem Soc* **2019**, *141*, 5231-5240. [<https://doi.org/10.1021/jacs.8b12101>]
2. Heel, A.; Holtappels, P.; Hug, P.; Graule, T. Flame spray synthesis of nanoscale $\text{La}_{0.6}\text{Sr}_{0.4}\text{Co}_{0.2}\text{Fe}_{0.8}\text{O}_{3-\delta}$ and $\text{Ba}_{0.5}\text{Sr}_{0.5}\text{Co}_{0.8}\text{Fe}_{0.2}\text{O}_{3-\delta}$ as cathode materials for intermediate temperature solid oxide fuel cells. *Fuel Cells* **2010**, *10*, 419-432. [<https://doi.org/10.1002/fuce.200900093>]
3. Fabbri, E.; Nachtegaal, M.; Binner, T.; Cheng, X.; Kim, B.J.; Durst, J.; Bozza, F.; Graule, T.; Schaublin, R.; Wiles, L., *et al.* Dynamic surface self-reconstruction is the key of highly active perovskite nanoelectrocatalysts for water splitting. *Nat Mater* **2017**, *16*, 925-+. [<https://doi.org/10.1038/Nmat4938>]
4. Clark, A.H.; Imbao, J.; Frahm, R.; Nachtegaal, M. Proqexafs: A highly optimized parallelized rapid processing software for qexafs data. *J Synchrotron Radiat* **2020**, *27*. [<https://doi.org/10.1107/S1600577519017053>]
5. Sheng, W.; Gasteiger, H.A.; Shao-Horn, Y. Hydrogen oxidation and evolution reaction kinetics on platinum: Acid vs alkaline electrolytes. *J Electrochem Soc* **2010**, *157*, B1529. [<https://doi.org/10.1149/1.3483106>]
6. Rheinlander, P.; Henning, S.; Herranz, J.; Gasteiger, H.A. Comparing hydrogen oxidation and evolution reaction kinetics on polycrystalline platinum in 0.1 M and 1 M KOH. *ECS Transactions* **2013**, *50*, 2163-2174. [<https://doi.org/10.1149/05002.2163ecst>]
7. Rheinländer, P.J.; Herranz, J.; Durst, J.; Gasteiger, H.A. Kinetics of the hydrogen oxidation/evolution reaction on polycrystalline platinum in alkaline electrolyte reaction order with respect to hydrogen pressure. *J Electrochem Soc* **2014**, *161*, F1448-F1457. [<https://doi.org/10.1149/2.0501414jes>]